



Article

Key Factors Affecting Carbon-Saving Intensity and Efficiency Based on the Structure of Green Space

Guohao Zhang¹, Chenyu Du^{2,3,*}  and Shidong Ge^{2,*} 

¹ School of Information Science and Engineering, Lanzhou University, Lanzhou 730000, China; zhanggh21@lzu.edu.cn

² College of Landscape Architecture and Art and International Union Laboratory of Landscape Architecture, Henan Agricultural University, Zhengzhou 450002, China

³ Department of Landscape Planning and Regional Development, Institute of Landscape Architecture, Urban Planning and Garden Art, Hungarian University of Agriculture and Life Sciences, 1118 Budapest, Hungary

* Correspondence: chenyu3051@gmail.com (C.D.); shidongge@henau.edu.cn (S.G.)

Abstract: Urban green spaces (UGSs) play a critical role in regulating global carbon cycling and mitigating the increase in atmospheric CO₂ concentrations. Research increasingly demonstrates that UGSs not only sequester carbon through photosynthesis but also effectively save carbon emissions by mitigating the urban heat island (UHI) effect. However, understanding the carbon-saving capacity (CSC) and the role of landscape patterns of UGSs in warming cities remains limited. Therefore, we have evaluated the carbon-saving capacity of UGSs in the main urban area of Shangqiu City by utilizing high-resolution remote sensing data and machine learning techniques. The study has focused on green patches larger than 10,000 m² and has analyzed the influence of landscape patterns of UGSs on carbon saving intensity (CSI) and carbon saving efficiency (CSE). The results reveal that the total CSI and the average CSE of UGSs are 7716 t CO₂ and 2.9 t CO₂ ha⁻¹ in Shangqiu, respectively. Landscape patterns of UGSs can explain 82% and 64% of the variability in CSI and CSE variance, respectively. Specifically, green space area is the critical determinant of CSI and CSE, followed by the perimeter–area ratio, shape index, and fractal dimension of UGSs. Therefore, this study advocates for the strategic integration of UGSs into city planning, emphasizing their spatial distribution and configuration to maximize their cooling and carbon-saving capacity.



Citation: Zhang, G.; Du, C.; Ge, S. Key Factors Affecting Carbon-Saving Intensity and Efficiency Based on the Structure of Green Space. *Land* **2024**, *13*, 1297. <https://doi.org/10.3390/land13081297>

Academic Editor: Muhammad Shafique

Received: 9 July 2024

Revised: 5 August 2024

Accepted: 14 August 2024

Published: 16 August 2024



Copyright: © 2024 by the authors. Licensee MDPI, Basel, Switzerland. This article is an open access article distributed under the terms and conditions of the Creative Commons Attribution (CC BY) license (<https://creativecommons.org/licenses/by/4.0/>).

Keywords: green space; carbon saving capacity; high-resolution remote sensing; machine learning; Shangqiu

1. Introduction

Urbanization has led to the widely recognized phenomenon of the urban heat island (UHI) effect [1,2]. The adverse impacts of UHI significantly harm the health of urban residents [3–6]. Urban planners must consider the complex relationship between rapid urbanization and UHI to ensure the sustainability of urban ecosystems [7]. Despite their importance, urban green spaces (UGSs), which directly provide ecological value in urban areas, are often overlooked and under-researched [8]. UGSs play a crucial role in offering local services to residents and are seen as a natural solution for mitigating UHI [9]. UGSs are considered effective strategies for alleviating global warming and UHI because they provide shade and facilitate evapotranspiration, helping to save energy and reduce carbon emissions [9–13]. Utilizing UGSs for cooling is cost-effective, environmentally friendly, and politically acceptable [14,15]. Quantifying the energy or carbon saving capacity (CSC) of UGSs in terms of heat mitigation can help develop more sustainable, economical, and decentralized urban measures in the context of severe urban climate warming [16]. However, the influencing factors of urban CSC, such as area, shape, and configuration, remain

unclear. Thoroughly identifying the CSC of UGSs can scientifically guide sustainable urban planning to alleviate urban heat environments [17].

The CSC of UGSs due to heat mitigation has been confirmed by some previous studies. For instance, urban parks in the Yangtze River Economic Belt could reduce CO₂ emissions by 31,722.5 t CO₂, equivalent to 38 million kWh of cooling from artificial devices, offsetting 5.37% of daily fossil fuel carbon emissions [18]. Shangqiu City Park can reduce a total of 300.57 t CO₂ due to heat mitigation [19]. UGSs in 48 cities in China could reduce a total of 353,000 t CO₂ due to heat mitigation [20]. Identifying the driving factors behind the CSC of UGSs remains a critical issue in urban ecology [21,22]. Increasing the area of UGSs can directly enhance the cooling effect, thereby reducing carbon emissions [23]. Meanwhile, there are thresholds for the impact of the area on cooling effects and CSC, and these thresholds vary. For example, Zhiyu Xu's study on UGSs in Beijing has found that medium-sized green spaces have the optimal cooling effect [24]. Zhou et al. suggest that the optimal cooling threshold in some Chinese cities is 20 ha or more [25]. Additionally, the shape of UGSs significantly impacts their CSC. Studies conducted on parks inside the Yangtze River Economic Belt reveal that the UGS's design significantly influences the parks' CSC [18]. More complex park shapes can offer greater cooling effects [26]. Another study found that more regular-shaped UGSs can provide better cooling effects [27]. Therefore, identifying the driving factors of CSC at the urban scale is essential for effective heat mitigation. Furthermore, the growing demand for land makes it challenging to increase the area of UGSs directly [28]. As public awareness of climate change and the emphasis on ecological security in urban planning has been attached, opportunities emerge to improve existing UGSs or create new ones. Exploring the driving factors of CSC can maximize the benefits of limited UGSs, enhancing the efficiency of cities in addressing extreme heat-related risks [29].

The relationship between UGS characteristics and CSC is complex and multifaceted. Numerous new algorithms have been applied to elucidate this relationship [17]. Machine learning methods have gained significant attention in exploring the connection between UGS metrics and CSC due to their flexibility and high adaptability in addressing nonlinear regression problems [30–32]. With recent advancements in analytical methods, the nonlinear characteristics of UGS indicators, particularly the cooling effect and CSC of UGSs, have been increasingly explored [18]. While linear regression and machine learning have extensively studied both linear and nonlinear relationships, there remains a gap in understanding the interaction effects between UGS landscape metrics and CSC. The interaction effects indicate that for an influencing factor that acts as a moderator, its effect on CSC depends on other factors, i.e., the moderating effect of the moderated factor. A study has shown that the effect of some landscape structure indicators on land surface temperature receives enhancement or inhibition from other indicators, i.e., there is an interaction, and at the same time, this interaction varies with the magnitude of the influencing factor [33]. McCarty et al. have found that green space, residential, and commercial space have the greatest influence on the cooling effect of parks through the study of their interaction, and the relationship between these two can be explored in more detail based on the interaction [34]. The results of another study on Tianjin city have revealed that changes in land surface temperature are the result of combinations of multiple factors with nonlinear interactions and that both factors have enhanced their explanation of surface temperature after interaction [35]. Recently, the SHapley Additive exPlanations (SHAP) method has been used to effectively demonstrate the relationships between influencing factors and their impacts on predictions [36]. SHAP can better interpret results and optimize models by revealing the relative contributions of various factors compared to traditional regression models [37]. Therefore, the SHAP method, combined with Random Forest Regression (RFR), can continuously reveal the interactions between landscape patterns and effectively explain the contribution of key influencing factors to the CSC of UGSs.

In Shangqiu, a prominent city in central China, the growing demand for natural spaces has led to the development and planning of more UGSs. However, understanding how

these green spaces can contribute to carbon saving through heat mitigation and maximizing their potential remains a significant challenge for sustainable urban development. This study analyzes the data from 769 UGS patches in Shangqiu to quantify their CSC during the summer of 2020–2021. Our study aims to: (1) spatially quantify the CSC of UGSs; (2) identify potential landscape drivers affecting the CSC of UGSs; and (3) explore the role of interaction effects between landscape pattern metrics in moderating changes in CSC.

2. Materials and Methods

2.1. Study Area

Shangqiu is located at latitude $33^{\circ}43' \sim 34^{\circ}52'$ N and longitude $114^{\circ}49' \sim 116^{\circ}39'$ E in the eastern part of Henan Province, China (Figure 1). The city is one of the major birthplaces of Chinese civilization, spanning 10,704 ha. Shangqiu features distinct seasons, in addition to a mild continental monsoon climate that is semi-humid [38]. Its population grew from 7.35 million to 7.66 million between 2010 and 2023, while its GDP reached 310.9 billion yuan in that same year [39].

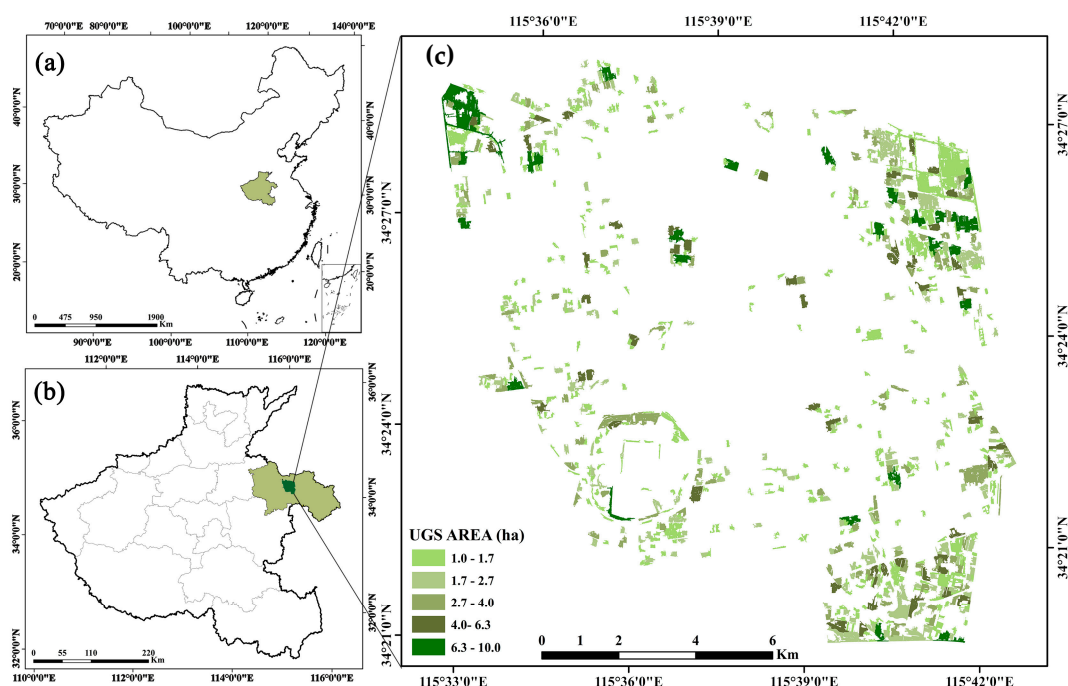


Figure 1. Location of the study area: (a) China, (b) Henan Province (light green) and Shangqiu City (dark green), and (c) the central area of Shangqiu with 769 urban green spaces.

To mitigate the negative impacts of urbanization, Shangqiu has been striving to become a forest and garden city. Numerous UGSs and city parks have been established, along with rural greening projects, mandatory tree planting, and forest and wetland restoration policies. Several national wetland parks have been constructed and are now in operation. The Minquan Yellow River Ancient Road Wetland has been included on the List of Wetlands of International Importance, making it one of China's 64 internationally significant wetlands [38]. For this study, we selected 769 UGSs within the main urban area of Shangqiu. Considering the additional cooling effect provided by nearby water bodies, we excluded any UGSs adjacent to water. To minimize interactions between UGSs, we have used a binning method. The selected UGSs are divided into 20 bins based on their area: Bin1: 1–1.04 ha, Bin2: 1.04–1.07 ha, Bin3: 1.07–1.12 ha, Bin4: 1.12–1.18 ha, Bin5: 1.18–1.23 ha, Bin6: 1.23–1.29 ha, Bin7: 1.29–1.36 ha, Bin8: 1.36–1.47 ha, Bin9: 1.47–1.56 ha, Bin10: 1.56–1.65 ha, Bin11: 1.65–1.8 ha, Bin12: 1.8–2.0 ha, Bin13: 2.0–2.2 ha, Bin14: 2.2–2.5 ha, Bin15: 2.5–2.8 ha, Bin16: 2.8–3.3 ha, Bin17: 3.3–4.0 ha, Bin18: 4.0–5.1 ha, Bin19: 5.1–9 ha, and Bin20: >9 ha.

2.2. Research Procedure and Data Source

As illustrated, this study follows four main steps: (1) Data Source: Landsat 8 OLI_TIRS satellite images are from Google Earth Engine (GEE) for the summers of 2020–2021 (June to September), selecting images with less than 10% cloud cover. Five Landsat remote sensing images are selected on 28 August 2020, 4 September 2020, 28 June 2021, 30 July 2021, and 16 September 2021, respectively. The classical Radiative Transfer Equation (RTE) is used to quantify the land surface temperature (LST) of Shangqiu City, and the average summer LST for each grid cell has been obtained. Furthermore, UGS in Shangqiu are extracted using GF-2 high-resolution imagery (0.8 m) through land use classification. (2) Data Processing: Green spaces smaller than 1 ha are excluded from this study due to the 30-m resolution of the LST data, and 769 green spaces are finally selected. Object-based image analysis and manual visual correction are applied to extract UGSs from the GF-2 imagery. (3) Variable Quantification: The average LST, carbon saving intensity, and carbon saving efficiency of each UGS are calculated based on their cooling boundaries. Additionally, 7 landscape pattern indices are computed using Fragstats 4.2 to assess potential influencing factors. These indices include Area (AREA), Perimeter (PERIM), Mean Radius of Gyration (GYRATE_MN), Mean Patch Area (PARA_MN), Mean Patch Shape Index (SHAPE_MN), Mean Fragment Shape Index (FRAC_MN), and Mean Related Circumscribing Circle (CIRCLE_MN), as shown in Table 1. (4) Relationship Identification: The RFR model combined with the Shapley additive explanations (SHAP) method was used to identify key factors influencing the CSC of UGSs (Figure 2).

Table 1. The explanation of the study’s use of landscape indexes.

Metrics	Abbreviation	Description
Area	Area	Area of each UGS
PERIM	PERIM	Perimeter of each UGS
Mean radius of gyration	GYRATE_MN	$GYRATE_{MN} = mean(GYRATE[patch_{ij}])$
Perimeter–Area Ratio Distribution	PARA_MN	$PARA_{MN} = mean(PARA[patch_{ij}])$
Shape Index Distribution	SHAPE_MN	$SHAPE_{MN} = mean(SHAPE[patch_{ij}])$
Mean Fractal Dimension Index	FRAC_MN	$FRAC_{MN} = mean(FRAC[patch_{ij}])$
Mean of related circumscribing circle	CIRCLE_MN	$CIRCLE_{MN} = mean(CIRCLE[patch_{ij}])$

$GYRATE[patch_{ij}]$: The radius of gyration of each UGS; $PARA[patch_{ij}]$: The perimeter area ratio of each UGS; $SHAPE[patch_{ij}]$: The shape index of each UGS; $FRAC[patch_{ij}]$: The fractal dimension index of each UGS. $CIRCLE[patch_{ij}]$: The related circumscribing circle of each UGS.

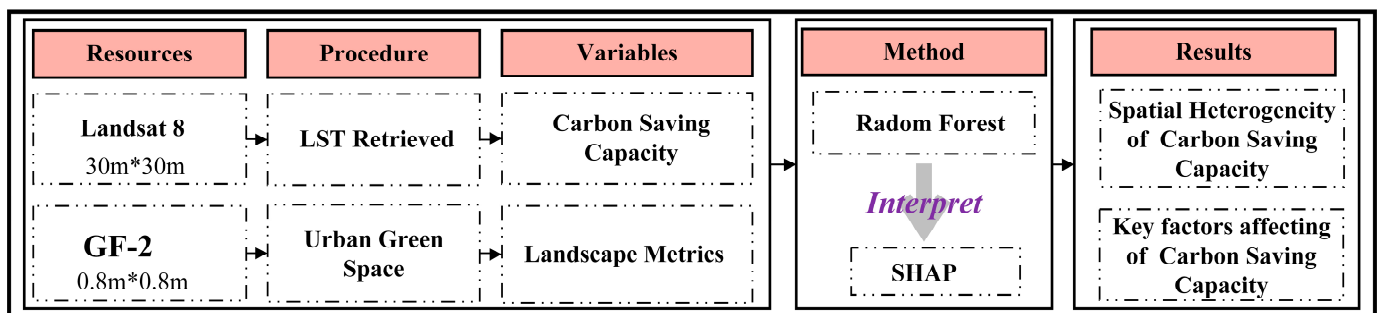


Figure 2. Research workflow of this study.

2.3. Methods

2.3.1. Calculating Carbon Saving Capacity and Extracting of UGS

The carbon-saving capacity of UGSs due to heat mitigation is estimated as the amount of CO₂ emissions that will be necessary to achieve equivalent cooling effects in the absence of UGSs. The carbon-saving capacity of UGSs is defined as the product of CSI and CSE. Drawing from previous studies [24,40], an area-adaptive method is utilized to define the cooling distance of each UGS. Assuming UGSs are circular, the cooling distance is defined as a buffer area approximately equal to the UGS area (Figure 3). The area-adaptive method resolves issues combined with using inflection point methods to determine cooling distances for small UGSs [25], and it avoids the pitfalls of applying fixed thresholds to UGSs of varying sizes [41]. The calculation formula is as follows:

$$P = (\sqrt{2} - 1) \times \sqrt{\frac{A}{\pi}} \quad (1)$$

where, P and A represent the buffer distance and the area of the UGS, respectively.

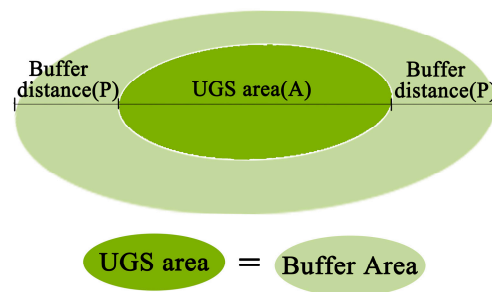


Figure 3. Illustration of the area-adaptive method.

This study employs the slice carbon saving model proposed by existing works to calculate CSI and CSE [18,42]. The formula is as follows:

$$CSI = \alpha \times \int_0^H \sum_{i=0}^N \frac{1}{3} (S_i + S_{i+1} + \sqrt{S_i S_{i+1}}) \Delta T \times h \quad (2)$$

here, α represents the product of the specific heat capacity of air (1004.68 J kg⁻¹ °C⁻¹), air density (1.2923 kg m⁻³), and coal consumption per unit of electricity generated (841 g/3.6 MJ) [18]. The horizontal influence distance is denoted by h (70 m) [42]. The basis zones are S_i and S_{i+1} , and the temperature difference between adjacent buffer zones is represented by ΔT . Finally, CSE is calculated as CSI divided by UGS area.

The information on UGSs in this study is extracted from GF-2 remote sensing imagery with a resolution of 0.8 m on 10 August 2021. To delineate the distribution of green spaces in Shangqiu City, an object-based classification method is employed in ENVI 5.3. This approach is enhanced by optimizing samples using high-resolution imagery from Google Earth in 2021, and further refined through expert visual inspection to minimize errors in land use data. The extraction results of UGSs in Shangqiu are shown in Figure 1c.

2.3.2. Random Forest Regression

The present research has used an RFR model to examine the link between CSC and potential affecting factors. Random Forest is a machine learning algorithm based on individual decision trees that is widely used in environmental and ecological research [43–45]. Compared to traditional linear regression models, RFR is more robust against multicollinearity and interaction effects among independent variables. It is less sensitive to outliers and noise in the dataset, making overfitting less likely [46]. For the same dataset, RFR demonstrates

higher accuracy compared to other traditional regression models [47,48]. In this study, RFR is implemented using the “randomForest” and “caret” packages in R 4.2.1.

2.3.3. Shapley Additive Explanation (SHAP)

This study utilizes the SHAP method alongside RFR to elucidate the relationship between potential influencing factors and CSC. By computing each factor’s SHAP value, SHAP successfully addresses the “black box” issue that arises with machine learning regression models by quantifying each factor’s impact on the final result. It identifies the relative contribution of each factor to the CSC [36,49]. SHAP is a game theory-based additive attribution algorithm. The factor’s impact on saving carbon emissions becomes more substantial as the absolute SHAP value increases [50]. The calculation formula for SHAP feature attributions is as follows:

$$\varnothing_j = \sum_{S \subseteq \{x_1, \dots, x_p\} \setminus \{x_j\}} \frac{|S|!(p - |S| - 1)!}{p!} (f_x(S \cup \{x_j\}) - f_x(S)) \quad (3)$$

here, \varnothing_j stands for the contribution of the j -th influencing factor, x is the vector of influencing factor values for the instance being explained, and p is the number of influencing factors. $f_x(S)$ denotes the prediction value for the subset S , where features not included in S are marginalized [37,51]. SHAP values are computed based on an additive feature attribution method, as expressed by the following formula:

$$g(z) = \varnothing_0 + \sum_{j=1}^M \varnothing_j z_j \quad (4)$$

here, g represents the explanatory model, z indicates the presence of a factor, M is the number of factors, and \varnothing_j is the model coefficient, representing the attribution of the j -th factor to the model prediction [36]. \varnothing_0 is a constant, indicating the expected value of the model prediction [52].

In this study, global SHAP values are used to express the overall importance of each factor, while local SHAP interpretability identifies the most critical factors affecting the CSC of UGSs [34]. Negative SHAP values represent a negative influence on CSC, whilst positive values show a beneficial effect. Additionally, SHAP interaction values are employed to elucidate the interaction effects of influencing factors on CSC.

3. Results

3.1. The Heterogeneity of UGS’s CSC

In Shangqiu City, the 769 UGSs collectively have contributed to a saving of 7716 t CO₂ emissions. Specifically, the total area of UGSs was 1973 ha, with CSI values ranging from 0.05 to 293.66 t CO₂. On average, each UGS has mitigated 10.03 t CO₂ emissions by alleviating UHI. Spatially, UGSs with higher CSI values are predominantly situated on the outskirts of the city, while those in the city center generally display lower CSI values. The UGSs with significant CSI are primarily located in the northwest and northeast parts of Shangqiu. The CSE of UGSs ranged from 0.004 to 10.44 t CO₂ ha⁻¹, with an average CSE of 2.9 t CO₂ ha⁻¹. There is evident spatial heterogeneity in the distribution of CSE, with higher values concentrated within the urban core and lower values more prevalent on the urban periphery (Figure 4a,b).

The frequency plot analysis has shown that the CSI of the green space in Shangqiu City is highly variable. The CSI is mainly distributed in 0~20 t CO₂, with a total of 687, accounting for 89% of the total (Figure 4c). Compared with CSI, CSE was more evenly distributed. CSE was mainly distributed in 0~5 t CO₂ ha⁻¹, totaling 651, accounting for 85%. As the value of CSE increases, the number of UGSs decreases gradually (Figure 4d).

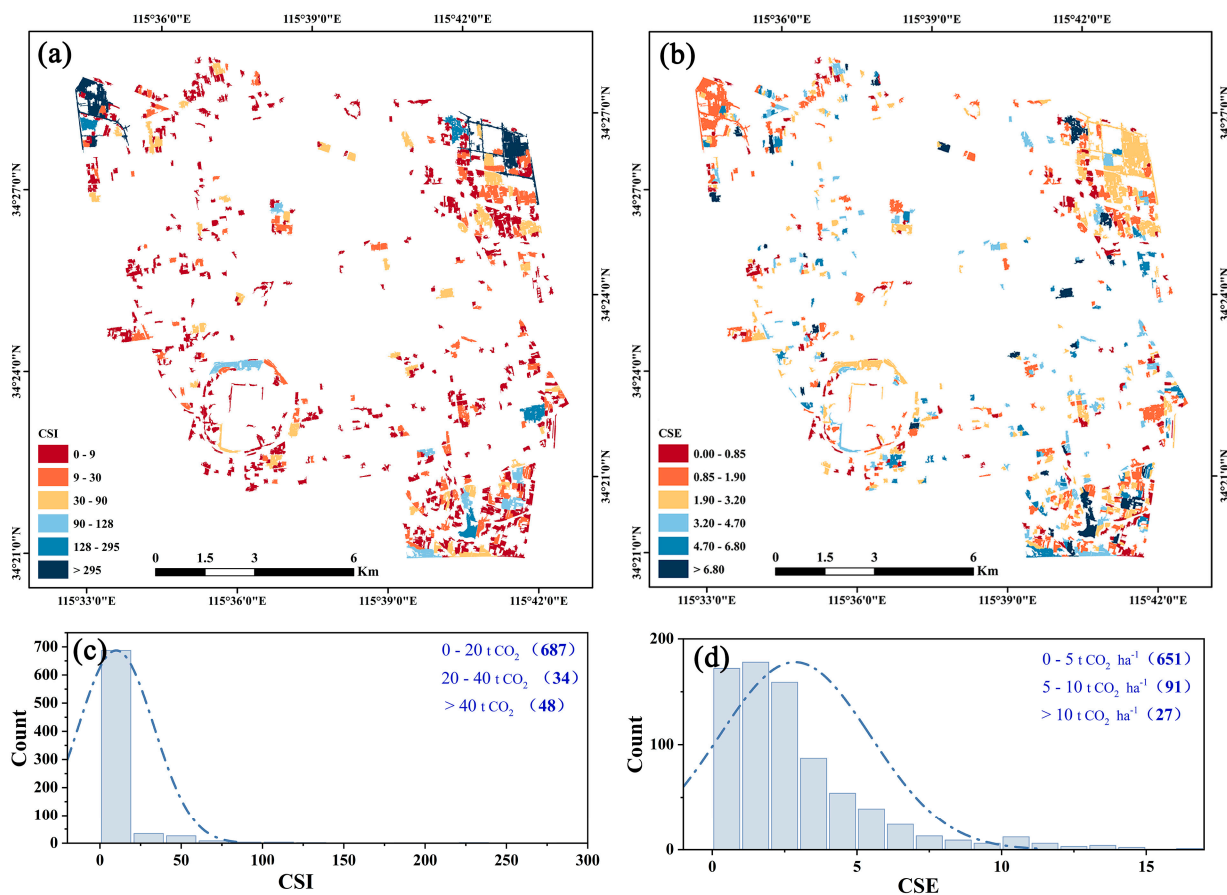


Figure 4. Spatial distribution and frequency plot of CSI and CSE. (a,c) CSI ($t\ CO_2$); (b,d) CSE ($t\ CO_2\ ha^{-1}$).

As the area of UGSs expanded, CSI generally exhibited a linear growth trend ($R^2 = 0.66$) (Figure 5). UGSs of comparable sizes have displayed significant heterogeneity in CSI. For instance, a 16 ha UGS has a CSI of 235.5 $t\ CO_2$, while a 33 ha UGS has a 98.97 $t\ CO_2$, indicating a difference of 136.53 $t\ CO_2$. These differences are less noticeable in UGS areas smaller than 5 ha. However, as the size of UGSs increased, the variability in CSI has become more apparent. Further binning analysis has illustrated the relationship between the CSI of UGSs (5th percentile, 95th percentile, and mean values) and their respective areas (Figure 5c). The results have demonstrated a stronger positive correlation ($R^2 = 0.99$) between CSI and the UGS area, with CSI values escalating from 1.68 $t\ CO_2$ in Bin 1 to 82.42 $t\ CO_2$ in Bin 20. Moreover, the heterogeneity of CSI has become more pronounced with the increase in area, especially in larger UGSs. The largest observed difference in CSI within Bin 20 can reach up to 292.21 $t\ CO_2$.

In contrast to CSI, the CSE has exhibited a weaker correlation with the UGS area (Figure 5). Similar to CSI, CSE has displayed significant heterogeneity even among UGSs of identical size. For example, the largest UGS (33 ha) has a CSE value of 2.97 $t\ CO_2\ ha^{-1}$, while a 1.6 ha UGS has a CSE value of 12.95 $t\ CO_2\ ha^{-1}$, representing a difference of 4.3 times (9.98 $t\ CO_2\ ha^{-1}$). Furthermore, higher CSE values are more common in smaller UGSs (>10 ha). This study has identified 28 UGSs with high CSE (<10 $t\ CO_2\ ha^{-1}$), 25 of which are smaller than 10 ha, accounting for 89% of the total. However, further binning analysis has revealed that the variability of CSE with respect to UGS area is more pronounced and did not necessarily increase with area. For instance, the difference in CSE was larger in Bin 5 (8.75 $t\ CO_2\ ha^{-1}$) than in Bin 16 (8.01 $t\ CO_2\ ha^{-1}$). Additionally, an exploration of the relationship between CSE (5th percentile, 95th percentile, and mean values) and UGS area (Figure 5d) has indicated a weak overall positive correlation between UGS area and the mean value of each bin, despite significant fluctuations. These results have underscored the strong

influence of internal structure within UGSs on CSE and have highlighted the potential for significant enhancement of UGS carbon sequestration capabilities through thoughtful and scientifically informed landscape planning.

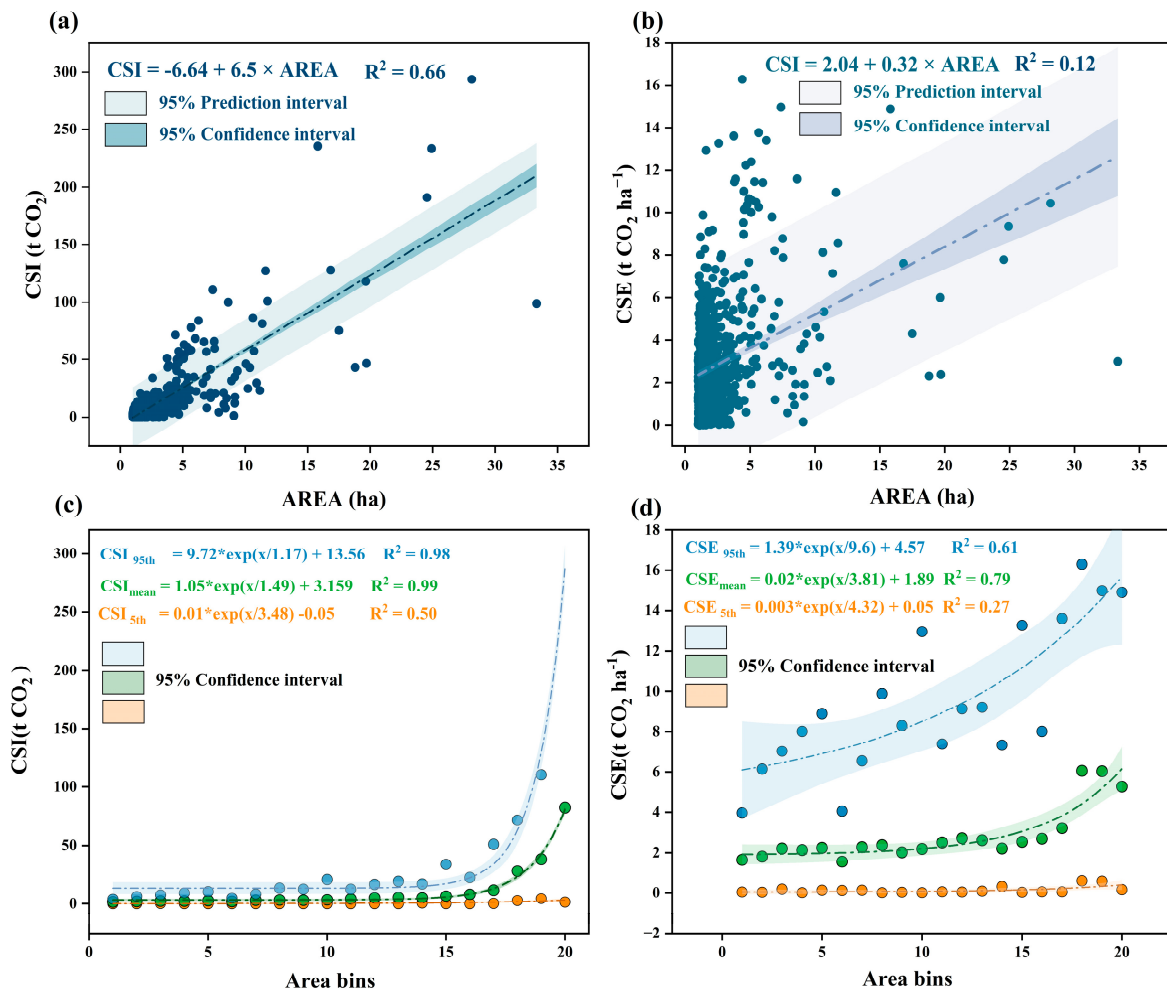


Figure 5. The scatter plot depicting the relationship between UGS area and CSI (a) and CSE (b); The 5th (blue line), mean (green dots), and 95th (orange line) of CSI (c) and CSE (d) along the 20 area bins of 769 urban green spaces. The ranges of area bins are: Bin1: 1–1.04, Bin2: 1.04–1.07, Bin3: 1.07–1.12, Bin4: 1.12–1.18, Bin5: 1.18–1.23, Bin6: 1.23–1.29, Bin7: 1.29–1.36, Bin8: 1.36–1.47, Bin9: 1.47–1.56, Bin10: 1.56–1.65, Bin11: 1.65–1.8, Bin12: 1.8–2.0, Bin13: 2.0–2.2, Bin14: 2.2–2.5, Bin15: 2.5–2.8, Bin16: 2.8–3.3, Bin17: 3.3–4.0, Bin18: 4.0–5.1, Bin19: 5.1–9, and Bin20: >9 (ha).

3.2. Relationships between Carbon-Saving Capacity and Landscape Influencing Factors

The Pearson correlation coefficients, which show the relationship between Landscape Indices and CSC, are visualized in Figure 6. The CSI shows a significant positive correlation with AREA (0.90), indicating that larger UGSs can notably enhance CSI. CSE is also positively correlated with AREA, but the correlation is weaker compared to CSI (0.48). Furthermore, there is a substantial positive correlation between CSI and CSE and the SHAPE and PERIM indices. This shows that the irregularly shaped green spaces can enhance the cooling effect of green spaces on the atmosphere around them, hence improving UGS’s capacity to reduce carbon emissions. The GYRATE positively has influenced both CSI and CSE, suggesting that a more compact arrangement of UGS patches significantly has enhanced their capacity for cooling and CSC. In contrast, the PARA negatively impacts both CSI and CSE, indicating that reducing this ratio can notably increase the CSC of UGSs. Moreover, the FRAC has correlated positively with CSI (0.24) and CSE (0.12),

which indicates that higher complexity in the configuration of UGS patches has enhanced the CSC.

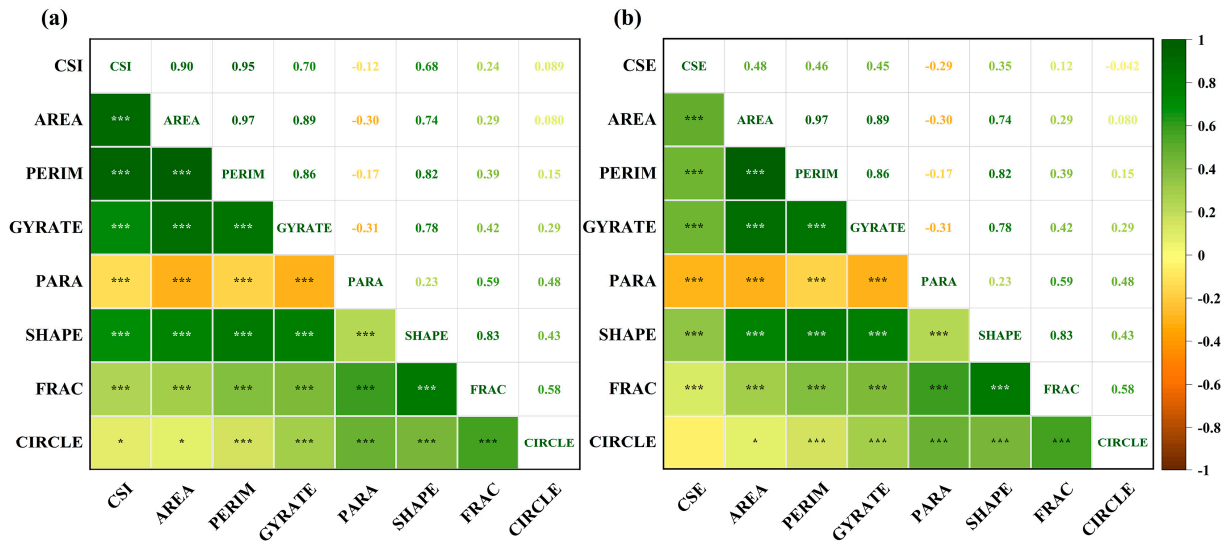


Figure 6. Correlation heatmaps between landscape patterns and CSI (a) and CSE (b). The number and stars show the significance level of coefficient, *** $p < 0.001$, * $p < 0.05$.

In the RF regression model for CSI and CSE, seven key landscape factors can explain 82% and 64% of the variance. The SHAP method is used to analyze the global SHAP value of each factor (Figure 7). Our findings indicated that the most significant factor influencing CSI and CSE is AREA (SHAP = 14326 and 0.31), accounting for 49.5% and 54.6% of the model, respectively. FRAC, SHAPE, and GYRATE are the following configuration metrics of green space, contributing 25.1%, 11.9%, and 8.1% of the CSI variations, respectively. PARA, SHAPE, GYRATE, and PERIM are the following configuration metrics to CSE, with contribution rates of 11.8%, 9.6%, 7.8%, and 7.6%, respectively. The factors with the least influence on CSI variations are PARA and CIRCLE, and together, they have shared only 2.8% of the total variability. Meanwhile, CIRCLE and FRAC are the least factors, accounting for 8.6% of the CSE variations.

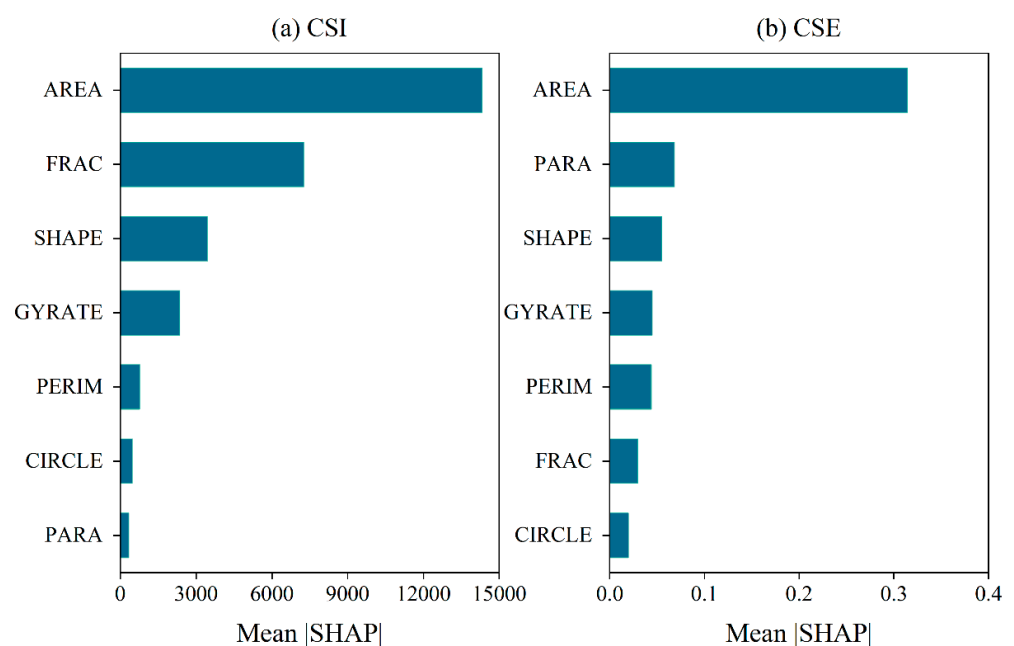


Figure 7. Relative importance of landscape metrics for CSI (a) and CSE (b).

3.3. Responses of CSI and CSE to the Configuration Metrics of UGS

In order to quantify the response of the UGS patch structure to its CSC, we have analyzed the relationship between each UGS index and the corresponding importance of CSI and CSE and have drawn a dependency diagram (Figure 8). For the AREA, 87.1% of the SHAP values are less than 0, indicating a predominantly negative impact of patch size on both CSI and CSE. The negative influence of the AREA on CSI and CSE stabilized when the area reached 3.66 ha and 5.03 ha, respectively, marking these values as potential turning points. For the GYRATE, 70.7% of the SHAP values for CSI are less than 0, while 64% of the SHAP values for CSE are greater than 0. This has suggested a negative overall effect of GYRATE on CSI and a positive overall effect of GYRATE on CSE, with respective turning points observed at 60 and 90. For the PERIM, 86.2% of the SHAP values for CSI are less than 0, while 53% of the SHAP values for CSE are greater than 0. Inflection points are observed at 2500 m and 1600 m. Similarly, the CIRCLE has affected CSI and CSE at critical points of 0.55 and 0.52, respectively. For the PARA, the critical points impacting CSI and CSE are found to be 690 and 565, respectively. Notably, the FRAC and SHAPE do not exhibit any critical points for either CSI or CSE, but the impact of this metric on CSI is negative.

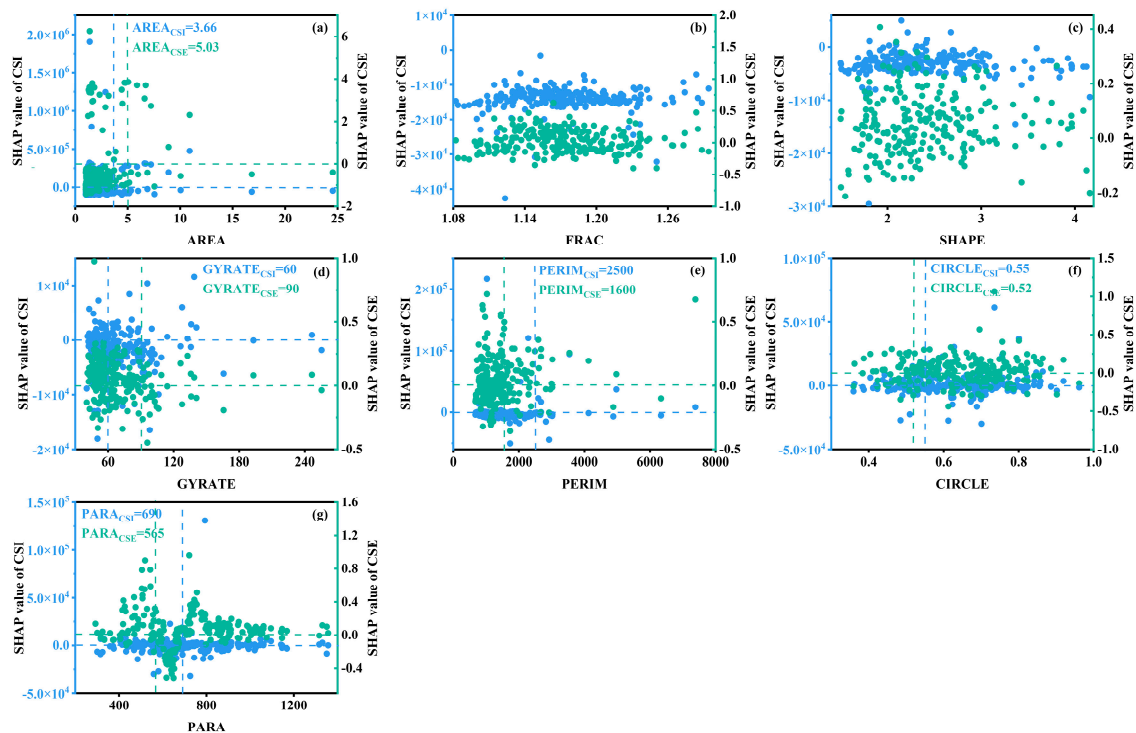


Figure 8. Dependency plots using the SHAP value of CSI and CSE for the seven UGS landscape metrics: AREA (a), FRAC (b), SHAPE (c), GYRATE (d), PERIM (e), CIRCLE (f), PARA (g).

3.4. Interactions between the Configuration Metrics of UGS

The interaction between indicator pairs demonstrated a significant relationship between the effect of AREA on CSI and the metrics PERIM, GYRATE, and PARA (Figure 9). As AREA has increased, the corresponding increase in PERIM, GYRATE, and PARA metrics has raised the interaction value from $-90,000$ to $-10,000$, suggesting that PERIM, GYRATE, and PARA may inhibit the CSC of AREA. Conversely, an increase in the metrics SHAPE, FRAC, and CIRCLE can potentially enhance the CSC of AREA. When the values of SHAPE, FRAC, and CIRCLE exceeded 700, 2.3, and 1.17, respectively, an increase in PARA reduced the interaction value to 0, implying that SHAPE, FRAC, and CIRCLE were the primary factors promoting PARA. The interaction of each parameter with PERIM and SHAPE exhibited a pattern opposite to that of AREA. The impacts of the metrics CIRCLE, FRAC, and GYRATE on CSI, in relation to the other parameters, are illustrated in Figures S2–S6.

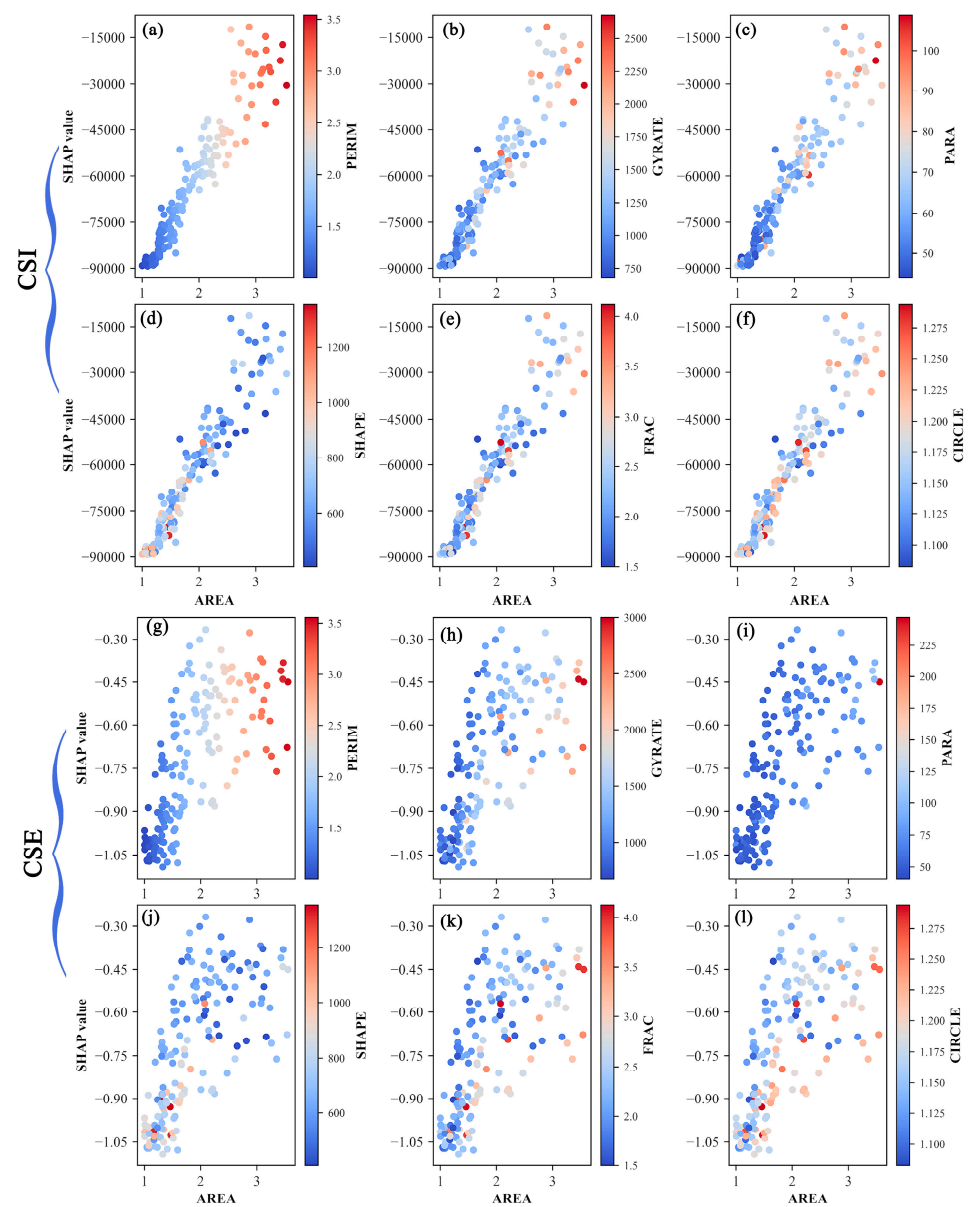


Figure 9. The dependence plot for landscape metrics using the SHAP interaction value. CSI (a–f), CSE (g–l).

The influence of AREA on CSE is as significant as its relation to PERIM, GYRATE, and PARA, albeit to a slightly different degree compared to CSI (Figure 9). As AREA has increased, the corresponding rise in PERIM, GYRATE, and PARA metrics elevated the interaction value from -1.1 to -0.2 , potentially suppressing the CSC of AREA. Simultaneously, an increase in the metrics SHAPE, FRAC, and CIRCLE can also enhance the CSC of AREA. When the values of PARA, SHAPE, and CIRCLE have exceeded 900, 3.0, and 1225, respectively, the role of FRAC in promoting carbon emission saving in green spaces is diminished. The interactions among the remaining parameters are depicted in Figures S2–S6.

4. Discussion

4.1. Comparison of CSC of UGS

Our results have indicated that the average CSE of UGSs in Shangqiu is $2.90 \text{ t CO}_2 \text{ ha}^{-1}$, surpassing findings from studies on Shangqiu City parks and parks in the Chinese Yangtze River Economic Belt (Table 2). The discrepancies can be explained by the following considerations. Firstly, the amount and proportion of small-scale UGSs may be a contributing

factor. Previous studies have identified a total of 118 parks in Shangqiu City, with 99 of them being smaller than 10 ha, constituting 84% of all parks [19]. In contrast, this study has encompassed 769 UGSs, with 755 of them being smaller than 10 ha, accounting for 98% of the total. Existing research has demonstrated a close relationship between the UGS scale and CSE. For instance, studies by Mo Chen et al. have shown higher CSE in small UGSs [18]. Weng Lin's research on UGSs in Beijing similarly suggested that smaller UGSs exhibit better CSE [42]. Jian Peng et al.'s findings indicated that smaller UGSs have a greater cooling intensity, corresponding to higher CSE [53]. Previous studies on Shangqiu City parks also has highlighted that small parks generally exhibit higher CSE compared to medium and large parks [19]. Secondly, the exclusion of water bodies may lead to differences in CSE. This study has employed a more precise method to quantify the CSC of UGSs by excluding water bodies during LST calculations. In contrast, previous studies on Shangqiu's parks did not exclude water bodies. The cooling effect of water bodies has been extensively proven by scholars [54–57]. Therefore, water bodies significantly have lowered the average temperature of UGSs, increasing the temperature difference with the surrounding environment and thus contributing to slightly higher CSE in this study compared to those studies on Shangqiu's parks.

Table 2. Average Carbon Savings Efficiency in different regions.

City or Region	Carbon Savings Efficiency (t CO ₂ ha ⁻¹)	Source
Shangqiu Urban Green Space (771)	2.90	This study
Shangqiu City Park (118)	1.79	[19]
The Yangtze River Economic Belt City Park (1510)	1.08	[18]
Köppen's subtropical humid climate	1.09	
Köppen's subtropical monsoon humid climate	0.91	
Yangtze River Delta urban agglomeration	1.2	
Cheng-Yu urban agglomeration	0.95	[18]
Middle-Reach Yangtze River urban agglomeration	0.89	
Shaxing City	1.6	
Meishan City	0.26	

In detail, the CSEs of UGSs in Shangqiu City are all higher than the results of the two climate zones, three city agglomerations, and other cities studied by the previous researchers (Table 2). This difference may also be due to the calculation method and study objectives. In other words, definitions of cooling effects and threshold distances of UGSs may also contribute to differences in CSE. Xin Cao et al. have used a fixed buffer zone of 500 m to quantify park cooling effects [41]. Wenqi Lin et al. have equated the calculation of UGS cooling intensity to that of lake basins, thereby defining the cooling intensity of UGSs as equivalent to the watershed area of lakes [58]. Mo Chen has considered the inflection point of LST around the buffer zone surrounding UGSs as the cooling boundary, resulting in different cooling boundaries for each UGS [18]. Chi-Ru Chang et al. have defined the cooling range of UGSs as the distance equivalent to one UGS width from the UGS, which is also the method used in our research [40]. Moreover, variations in CSE can be caused by variations in the study subjects. This study has focused on UGSs, whereas previous studies focused on urban parks [19]. The cooling effects of both have been confirmed by many studies [11,24,59,60]. However, parks have duties such as providing activity and service facilities for urban residents, including squares, sports fields, and roads. According to China's park design guidelines, parks must have at least 65% green space, which allows for the arrangement of 35% of impermeable surfaces. Parks have lower CSE compared to UGSs because impermeable surfaces greatly raise LST and decrease the temperature differential between them and the surrounding area [61,62]. Most previous studies have focused on parks, but in China, parks are only part of the UGS [18,19,42]. Therefore, a large number of green areas and urban forests have been neglected. Few studies have comprehensively

investigated the CSC of all green spaces in the city. Our work quantifies the CSC of all UGSs in the city, which has an important impact on the shift from “Quantity increase” to “Quality improvement” of UGSs.

In addition, our results show that high CSE values are mostly distributed in the inner part of the city, but high CSI values are mostly distributed in the outer part of the city. This may be related to the distribution characteristics and planning strategies of UGSs. The distribution of UGSs in Shangqiu City has the characteristics of a small area and a small number in the city center, and a large number and a large area in the city periphery (Figure 1c). The positive correlation between CSI and UGS areas and the higher CSE in small UGS areas has been widely confirmed [18,24,63,64]. In recent years, various cities in China have implemented afforestation policies to address urban climate issues. For example, Beijing has implemented afforestation policies such as the “Plain Afforestation Project” and “Planting Where Possible” [65]. However, due to the difficulty of directly increasing green space area within cities, most policies have prioritized afforestation in suburban areas far from the city center [17,66]. On the other hand, the UGS system planning of Shangqiu City is also one of the reasons. The UGS of Shangqiu is planned to be divided into three major zones based on the document “Shangqiu Master Plan (2015–2030)”, which are the Yellow River Ecological Zone (north), the Agroforestry Ecological Zone (east), and the Relic Ecological Zone (southwest) [67]. These three major UGS systems are located at the urban periphery. While the smaller scale parks and green spaces are planned to be distributed in spots in the city center. This indirectly reinforces the distributional characteristics of urban green spaces, which leads to significant spatial heterogeneity of CSI and CSE.

4.2. Impact of Landscape Structures on UGS's CSC

Overall, landscape patterns significantly influence the CSC of UGSs, aligning with previous CSC studies [18,19]. Specifically, this study has revealed that the CSI and CSE of UGSs are primarily influenced by the AREA indices, showing a significant positive correlation. This is consistent with the results of previous studies on urban green spaces in Beijing and parks in the Yangtze River Economic Belt. Wenqi Lin et al. showed a significant and direct positive correlation between the CSC and the area of UGS in their study of green spaces in Beijing [42]. The results of CSC studies on parks in the Yangtze River Economic Zone also showed that larger parks can significantly increase CSC values [18]. The SHAP analysis results indicate that the positive effect of area on CSI and CSE reaches a turning point when the green space area exceeds 3.66 ha and 5.03 ha, respectively. This suggests that larger UGSs tend to have higher CSC, and 5 ha is the minimum area for park design. This finding is consistent with Wenqi Lin et al.'s research on the CSC of UGSs in Beijing, which indicates a direct and significant relationship between CSC and UGS scale [42]. Some previous studies have indicated that as green space area increases, the cooling distance linearly increases while cooling intensity nonlinearly increases [68]. Larger patches of green space are more stable in terms of climate evolution than smaller areas and are more likely to provide effective cooling effects and CSC. Moreover, larger UGSs harbor more vegetation, leading to increased transpiration and shading effects, thereby enhancing cooling and elevating CSI values [10,64,69].

Additionally, PARA and SHAPE are identified as primary drivers of CSE in UGSs, showing a significant positive correlation. This result is consistent with the findings of Wenqi Lin et al. that the shape of the UGSs is directly and positively correlated with the CSC. The more complex the shape of the UGS, the longer the boundaries of the unit UGS, and thus more heat flows through these boundaries into the cooled UGS [42]. In other words, this is attributed to the ability of complex-shaped UGSs to enhance thermal connectivity with the surrounding environment, thereby improving cooling efficiency [18]. CSC studies of parks in the Yangtze River Economic Zone have similarly demonstrated the contribution of park shape to CSC, similar to the results of this study [18]. Currently, there are differing conclusions in prior studies regarding the relationship between the shape of UGSs and cooling effects. Some studies have suggested that regularly shaped UGSs exhibit better

cooling effects [27,70,71], while others indicate that more complex-shaped UGSs achieve superior cooling effects [69,72]. A study highlighted that increasing shape complexity in medium-sized UGSs positively impacts cooling effects, whereas regularly shaped UGSs in small or large sizes are more favorable for cooling effects [24]. Furthermore, a study in Israel suggested that the SHAPE Index of UGSs has almost no effect on the cooling effects [73]. Several reasons may account for these disparate results. Firstly, differences in temperature data sources can lead to varying outcomes. For instance, studies in Israel have used meteorological data from observation points, whereas some studies have relied on LST derived from remote sensing imagery. Differences between air temperature and LST have been documented in previous literature, where studies based on air temperature generally find greater cooling effects from trees compared to water bodies [74,75], whereas those based on land surface temperature often find greater cooling effects from water bodies than from trees [76,77]. Secondly, climate characteristics play a crucial role in generating different outcomes [78]. Previous studies often encompass cities located in diverse climatic regions, where varying climate conditions significantly influence UGS cooling intensity and the impact of landscape patterns on cooling effects [79,80]. In conclusion, cities represent complex human ecosystems, and most case-based studies yield diverse results due to distinct natural and economic conditions [81]. From another perspective, this underscores the necessity of conducting CSC studies on individual cities.

4.3. Implications for Urban Management and Planning

This study underscores the indispensable and pivotal role of UGSs in mitigating the UHI and indirectly contributing to the CSC [82]. In this context, urban planners must recognize green spaces as critical components of urban infrastructure, deserving equal attention alongside transportation networks and public service facilities [83]. Planners should integrate green spaces organically into the overall urban framework, particularly by expanding coverage in city centers and densely populated areas. While planning and constructing large-scale green patches on urban peripheries to maximize their cooling efficiency [26,84,85]. Achieving this goal requires enhancing the spatial precision of green space planning to ensure that each green patch can effectively capture and utilize its cooling potential [86].

Furthermore, this study reveals a close correlation between landscape pattern indices and CSC, emphasizing that the layout of UGSs profoundly influences their capacity to mitigate carbon emissions [18]. Urban planners can optimize the form, scale, and distribution of UGSs to enhance their CSC [87]. Specifically, designing green spaces with more complex shapes and higher perimeter-to-area ratios can significantly improve their cooling efficiency, thereby expanding their indirect CSC [69]. Additionally, the widespread adoption of high-resolution remote sensing technology and machine learning algorithms should be promoted to assess and predict the impact of different landscape configurations on CSC. This approach provides robust guidance for urban design by demonstrating the predictive capability of data-driven methods in urban planning. In this study, machine learning models successfully predicted the impact of landscape patterns on CSC, showcasing the substantial value of data-driven approaches in urban planning [43,46,88]. Planners should leverage these models to simulate various configurations of UGSs and their effects on temperature and carbon emissions, thereby identifying design solutions that maximize CSC. Furthermore, integrating real-time remote sensing data into urban planning processes can offer timely insights into the current status and effectiveness of existing green spaces, guiding adaptive management strategies effectively.

To fully harness the CSC of UGSs, it is crucial to develop supportive policies and promote widespread community engagement in sustainable urban greening efforts. Effective policies should incentivize individuals and groups to create and maintain green spaces. Community involvement is essential for ensuring these spaces are well-managed and for enhancing public awareness of their role in addressing climate change challenges [89]. Educational initiatives and participatory planning processes empower residents to participate

in urban greening efforts, foster a sense of ownership, and ensure the long-term success of these action plans.

4.4. Limitations and Uncertainties

Using the Random Forest model and SHAP algorithm, the influence of the UGS landscape pattern index on CSC is identified, highlighting the specific contribution of key factors to CSC, and confirming that the pattern and design of the UGS can significantly enhance CSC. However, there are still some limitations in this study that can be improved in future research. Firstly, only the landscape pattern index was used as an influencing factor on CSC, and the influence mechanism of CSC can be comprehensively explored in the future using a multidimensional approach. Among them, green space accessibility, green space maintenance cost, urban economic level, and population around the green space can be comprehensively investigated from the aspect of influence on CSC. Secondly, only LST images from 2020–2021 are used in this study, and a long-time series of UGSs can be investigated in the future using Google Earth Engine. Thirdly, the carbon sequestration capacity of the UGS can be combined with the CSC in the future to more comprehensively estimate the contribution of the UGS to the achievement of the carbon neutrality goal.

5. Conclusions

This study evaluated UGS's potential to save carbon emissions in Shangqiu City using machine learning techniques and high-resolution remote sensing data. The results of the study are as follows:

1. The findings demonstrate that UGSs contribute to CSC by alleviating the urban heat island effect. Specifically, the total CSI mitigated by UGSs in Shangqiu City amounts to 7716 t CO₂, with an average CSE of 2.9 t CO₂ ha⁻¹. These results underscore the critical role of UGSs in mitigating carbon emissions amidst rapid urbanization and exacerbated UHI.
2. There is a close relationship between landscape pattern indices and CSC in UGSs. The area of green spaces emerges as a crucial determinant of CSI and CSE, followed by perimeter–area ratio, shape index, and fractal dimension of UGSs. These findings show that optimizing UGS layout and design can significantly enhance their CSC.
3. Machine learning models, particularly RFR models, demonstrate strong predictive capabilities by explaining 82% of the variation for CSI and 64% for CSE. This underscores the value of data-driven approaches in urban planning and management.

The study provides clear suggestions for urban planning and policy: strategically integrate UGS into city structures, emphasizing their spatial distribution and configuration to maximize cooling and CSC. Encouraging community participation and implementing supportive policies are also crucial for promoting sustainable urban greening initiatives. Overall, this study provides empirical evidence of the CSC of UGSs and offers a methodological framework applicable to other urban environments. It contributes to the field by advocating for strategic UGS planning that fully considers their ecological and climatic benefits for urban sustainability and climate change mitigation.

Supplementary Materials: The following supporting information can be downloaded at: <https://www.mdpi.com/article/10.3390/land13081297/s1>, Figure S1. The dependence plot for landscape metrics (FRAC) using the SHAP interaction value. Figure S2. The dependence plot for landscape metrics (SHAPE) using the SHAP interaction value. Figure S3. The dependence plot for landscape metrics (GYRATE) using the SHAP interaction value. Figure S4. The dependence plot for landscape metrics (PERIM) using the SHAP interaction value. Figure S5. The dependence plot for landscape metrics (CIRCLE) using the SHAP interaction value. Figure S6. The dependence plot for landscape metrics (PARA) using the SHAP interaction value.

Author Contributions: Conceptualization, G.Z. and S.G.; methodology, G.Z., S.G. and C.D.; software, G.Z. and S.G.; validation, G.Z. and C.D.; formal analysis, S.G. and C.D.; investigation, S.G. and C.D.; resources, S.G. and C.D.; data curation, G.Z. and S.G.; writing—original draft preparation, G.Z., S.G.

and C.D.; writing—review and editing, G.Z., S.G. and C.D.; visualization, G.Z. and C.D.; supervision, S.G. and C.D.; project administration, C.D. and S.G.; funding acquisition, C.D. and S.G. All authors have read and agreed to the published version of the manuscript.

Funding: This study was supported by the Key Technology R&D Program of Henan Province (242102320320 and 232102320190) and the Special Fund for Young Talents in Henan Agricultural University (30500930 and 30501053).

Data Availability Statement: The data presented in this study are available on request from the corresponding author due to laboratory confidentiality agreements.

Conflicts of Interest: The authors declare no conflict of interest.

References

- Grimm, N.B.; Faeth, S.H.; Golubiewski, N.E.; Redman, C.L.; Wu, J.; Bai, X.; Briggs, J.M. Global Change and the Ecology of Cities. *Science* **2008**, *319*, 756–760. [[CrossRef](#)] [[PubMed](#)]
- Forman, R.T.T. Urban ecology principles: Are urban ecology and natural area ecology really different? *Landsc. Ecol.* **2016**, *31*, 1653–1662. [[CrossRef](#)]
- Yu, Z.; Yao, Y.; Yang, G.; Wang, X.; Vejre, H. Spatiotemporal patterns and characteristics of remotely sensed region heat islands during the rapid urbanization (1995–2015) of Southern China. *Sci. Total Environ.* **2019**, *674*, 242–254. [[CrossRef](#)]
- Ward, K.; Lauf, S.; Kleinschmit, B.; Endlicher, W. Heat waves and urban heat islands in Europe: A review of relevant drivers. *Sci. Total Environ.* **2016**, *569–570*, 527–539. [[CrossRef](#)]
- Ebi, K.L.; Capon, A.; Berry, P.; Broderick, C.; de Dear, R.; Havenith, G.; Honda, Y.; Kovats, R.S.; Ma, W.; Malik, A.; et al. Hot weather and heat extremes: Health risks. *Lancet* **2021**, *398*, 698–708. [[CrossRef](#)]
- Maggiotto, G.; Miani, A.; Rizzo, E.; Castellone, M.D.; Piscitelli, P. Heat waves and adaptation strategies in a mediterranean urban context. *Environ. Res.* **2021**, *197*, 111066. [[CrossRef](#)] [[PubMed](#)]
- Kotharkar, R.; Ghosh, A. Progress in extreme heat management and warning systems: A systematic review of heat-health action plans (1995–2020). *Sustain. Cities Soc.* **2022**, *76*, 103487. [[CrossRef](#)]
- Gaston, K.J.; Ávila-Jiménez, M.L.; Edmondson, J.L. REVIEW: Managing urban ecosystems for goods and services. *J. Appl. Ecol.* **2013**, *50*, 830–840. [[CrossRef](#)]
- Wong, N.H.; Tan, C.L.; Kolokotsa, D.D.; Takebayashi, H. Greenery as a mitigation and adaptation strategy to urban heat. *Nat. Rev. Earth Environ.* **2021**, *2*, 166–181. [[CrossRef](#)]
- Gunawardena, K.R.; Wells, M.J.; Kershaw, T. Utilising green and bluespace to mitigate urban heat island intensity. *Sci. Total Environ.* **2017**, *584–585*, 1040–1055. [[CrossRef](#)]
- Vulova, S.; Rocha, A.D.; Meier, F.; Nouri, H.; Schulz, C.; Soulsby, C.; Tetzlaff, D.; Kleinschmit, B. City-wide, high-resolution mapping of evapotranspiration to guide climate-resilient planning. *Remote Sens. Environ.* **2023**, *287*, 113487. [[CrossRef](#)]
- Zhao, L.; Lee, X.; Schultz, N.M. A wedge strategy for mitigation of urban warming in future climate scenarios. *Atmos. Chem. Phys.* **2017**, *17*, 9067–9080. [[CrossRef](#)]
- Li, D.; Liao, W.; Rigden, A.J.; Liu, X.; Wang, D.; Malyshev, S.; Shevliakova, E. Urban heat island: Aerodynamics or imperviousness? *Sci. Adv.* **2019**, *5*, eaau4299. [[CrossRef](#)] [[PubMed](#)]
- Carvalho, D.; Martins, H.; Marta-Almeida, M.; Rocha, A.; Borrego, C. Urban resilience to future urban heat waves under a climate change scenario: A case study for Porto urban area (Portugal). *Urban Clim.* **2017**, *19*, 1–27. [[CrossRef](#)]
- Martins, T.A.L.; Adolphe, L.; Bonhomme, M.; Bonneaud, F.; Faraut, S.; Ginestet, S.; Michel, C.; Guyard, W. Impact of Urban Cool Island measures on outdoor climate and pedestrian comfort: Simulations for a new district of Toulouse, France. *Sustain. Cities Soc.* **2016**, *26*, 9–26. [[CrossRef](#)]
- Yu, Z.; Yao, Y.; Yang, G.; Wang, X.; Vejre, H. Strong contribution of rapid urbanization and urban agglomeration development to regional thermal environment dynamics and evolution. *For. Ecol. Manag.* **2019**, *446*, 214–225. [[CrossRef](#)]
- Geng, X.; Yu, Z.; Zhang, D.; Li, C.; Yuan, Y.; Wang, X. The influence of local background climate on the dominant factors and threshold-size of the cooling effect of urban parks. *Sci. Total Environ.* **2022**, *823*, 153806. [[CrossRef](#)]
- Chen, M.; Jia, W.; Du, C.; Shi, M.; Henebry, G.M.; Wang, K. Carbon saving potential of urban parks due to heat mitigation in Yangtze River Economic Belt. *J. Clean. Prod.* **2023**, *385*, 135713. [[CrossRef](#)]
- Gao, J.; Han, H.; Ge, S. Carbon-Saving Potential of Urban Parks in the Central Plains City: A High Spatial Resolution Study Using a Forest City, Shangqiu, China, as a Lens. *Land* **2023**, *12*, 1383. [[CrossRef](#)]
- Qiu, K.; Jia, B. Carbon emission reduction from the cooling effect of urban greenspace in the three urban agglomerations in China. *Reg. Environ. Chang.* **2023**, *23*, 134. [[CrossRef](#)]
- Bowler, D.E.; Buyung-Ali, L.; Knight, T.M.; Pullin, A.S. Urban greening to cool towns and cities: A systematic review of the empirical evidence. *Landsc. Urban Plan.* **2010**, *97*, 147–155. [[CrossRef](#)]
- Du, H.; Cai, W.; Xu, Y.; Wang, Z.; Wang, Y.; Cai, Y. Quantifying the cool island effects of urban green spaces using remote sensing Data. *Urban For. Urban Green.* **2017**, *27*, 24–31. [[CrossRef](#)]

23. Wu, Z.; Chen, L. Optimizing the spatial arrangement of trees in residential neighborhoods for better cooling effects: Integrating modeling with in-situ measurements. *Landsc. Urban Plan.* **2017**, *167*, 463–472. [[CrossRef](#)]
24. Xu, Z.; Zhao, S. Scale dependence of urban green space cooling efficiency: A case study in Beijing metropolitan area. *Sci. Total Environ.* **2023**, *898*, 165563. [[CrossRef](#)] [[PubMed](#)]
25. Zhou, W.; Yu, W.; Wu, T. An alternative method of developing landscape strategies for urban cooling: A threshold-based perspective. *Landsc. Urban Plan.* **2022**, *225*, 104449. [[CrossRef](#)]
26. Qiu, K.; Jia, B. The roles of landscape both inside the park and the surroundings in park cooling effect. *Sustain. Cities Soc.* **2020**, *52*, 101864. [[CrossRef](#)]
27. Peng, J.; Xie, P.; Liu, Y.; Ma, J. Urban thermal environment dynamics and associated landscape pattern factors: A case study in the Beijing metropolitan region. *Remote Sens. Environ.* **2016**, *173*, 145–155. [[CrossRef](#)]
28. Seto, K.C.; Güneralp, B.; Hutyrá, L.R. Global forecasts of urban expansion to 2030 and direct impacts on biodiversity and carbon pools. *Proc. Natl. Acad. Sci. USA* **2012**, *109*, 16083–16088. [[CrossRef](#)] [[PubMed](#)]
29. Marando, F.; Heris, M.P.; Zulian, G.; Udías, A.; Mentaschi, L.; Chrysoulakis, N.; Parastatidis, D.; Maes, J. Urban heat island mitigation by green infrastructure in European Functional Urban Areas. *Sustain. Cities Soc.* **2022**, *77*, 103564. [[CrossRef](#)]
30. Han, L.; Zhao, J.; Gao, Y.; Gu, Z. Prediction and evaluation of spatial distributions of ozone and urban heat island using a machine learning modified land use regression method. *Sustain. Cities Soc.* **2022**, *78*, 103643. [[CrossRef](#)]
31. Zhao, W.; Duan, S.-B.; Li, A.; Yin, G. A practical method for reducing terrain effect on land surface temperature using random forest regression. *Remote Sens. Environ.* **2019**, *221*, 635–649. [[CrossRef](#)]
32. Zhou, L.; Hu, F.; Wang, B.; Wei, C.; Sun, D.; Wang, S. Relationship between urban landscape structure and land surface temperature: Spatial hierarchy and interaction effects. *Sustain. Cities Soc.* **2022**, *80*, 103795. [[CrossRef](#)]
33. Liu, Z.; Fu, L.; Wu, C.; Zhang, Z.; Zhang, Z.; Lin, X.; Li, X.; Hu, Y.; Ge, H. Spatialized importance of key factors affecting park cooling intensity based on the park scale. *Sustain. Cities Soc.* **2023**, *99*, 104952. [[CrossRef](#)]
34. McCarty, D.; Lee, J.; Kim, H.W. Machine Learning Simulation of Land Cover Impact on Surface Urban Heat Island Surrounding Park Areas. *Sustainability* **2021**, *13*, 12678. [[CrossRef](#)]
35. Hu, D.; Meng, Q.; Zhang, L.; Zhang, Y. Spatial quantitative analysis of the potential driving factors of land surface temperature in different “Centers” of polycentric cities: A case study in Tianjin, China. *Sci. Total Environ.* **2020**, *706*, 135244. [[CrossRef](#)] [[PubMed](#)]
36. Lundberg, S.; Lee, S.-I. A Unified Approach to Interpreting Model Predictions. *arXiv* **2017**. [[CrossRef](#)]
37. Hu, Y.; Wu, C.; Meadows, M.E.; Feng, M. Pixel level spatial variability modeling using SHAP reveals the relative importance of factors influencing LST. *Env. Monit Assess* **2023**, *195*, 407. [[CrossRef](#)]
38. Shangqiu Municipal People’s Government Basic Information of Shangqiu City. Available online: <https://www.shangqiu.gov.cn/sq> (accessed on 11 June 2024).
39. Shangqiu Statistical Yearbook 2023. Available online: https://www.sqxq.gov.cn/bmxxgk/sfqttj/jczwggk4543/tjly/tjsj4/sjfb/content_137478 (accessed on 11 June 2024).
40. Chang, C.-R.; Li, M.-H.; Chang, S.-D. A preliminary study on the local cool-island intensity of Taipei city parks. *Landsc. Urban Plan.* **2007**, *80*, 386–395. [[CrossRef](#)]
41. Cao, X.; Onishi, A.; Chen, J.; Imura, H. Quantifying the cool island intensity of urban parks using ASTER and IKONOS data. *Landsc. Urban Plan.* **2010**, *96*, 224–231. [[CrossRef](#)]
42. Lin, W.; Wu, T.; Zhang, C.; Yu, T. Carbon savings resulting from the cooling effect of green areas: A case study in Beijing. *Environ. Pollut.* **2011**, *159*, 2148–2154. [[CrossRef](#)]
43. Lyu, R.; Pang, J.; Tian, X.; Zhao, W.; Zhang, J. How to optimize the 2D/3D urban thermal environment: Insights derived from UAV LiDAR/multispectral data and multi-source remote sensing data. *Sustain. Cities Soc.* **2023**, *88*, 104287. [[CrossRef](#)]
44. Ossola, A.; Jenerette, G.D.; McGrath, A.; Chow, W.; Hughes, L.; Leishman, M.R. Small vegetated patches greatly reduce urban surface temperature during a summer heatwave in Adelaide, Australia. *Landsc. Urban Plan.* **2021**, *209*, 104046. [[CrossRef](#)]
45. Yao, X.; Zhu, Z.; Zhou, X.; Shen, Y.; Shen, X.; Xu, Z. Investigating the effects of urban morphological factors on seasonal land surface temperature in a “Furnace city” from a block perspective. *Sustain. Cities Soc.* **2022**, *86*, 104165. [[CrossRef](#)]
46. Li, Z.; Hu, D. Exploring the relationship between the 2D/3D architectural morphology and urban land surface temperature based on a boosted regression tree: A case study of Beijing, China. *Sustain. Cities Soc.* **2022**, *78*, 103392. [[CrossRef](#)]
47. Wu, Q.; Li, Z.; Yang, C.; Li, H.; Gong, L.; Guo, F. On the Scale Effect of Relationship Identification between Land Surface Temperature and 3D Landscape Pattern: The Application of Random Forest. *Remote Sens.* **2022**, *14*, 279. [[CrossRef](#)]
48. Logan, T.M.; Zaitchik, B.; Guikema, S.; Nisbet, A. Night and day: The influence and relative importance of urban characteristics on remotely sensed land surface temperature. *Remote Sens. Environ.* **2020**, *247*, 111861. [[CrossRef](#)]
49. Lundberg, S.M.; Erion, G.; Chen, H.; DeGrave, A.; Prutkin, J.M.; Nair, B.; Katz, R.; Himmelfarb, J.; Bansal, N.; Lee, S.-I. From local explanations to global understanding with explainable AI for trees. *Nat. Mach. Intell.* **2020**, *2*, 56–67. [[CrossRef](#)] [[PubMed](#)]
50. Fan, Y.V.; Jiang, P.; Tan, R.R.; Aviso, K.B.; You, F.; Zhao, X.; Lee, C.T.; Klemeš, J.J. Forecasting plastic waste generation and interventions for environmental hazard mitigation. *J. Hazard. Mater.* **2022**, *424*, 127330. [[CrossRef](#)] [[PubMed](#)]
51. Li, X.; Wu, C.; Meadows, M.E.; Zhang, Z.; Lin, X.; Zhang, Z.; Chi, Y.; Feng, M.; Li, E.; Hu, Y. Factors Underlying Spatiotemporal Variations in Atmospheric PM2.5 Concentrations in Zhejiang Province, China. *Remote Sens.* **2021**, *13*, 3011. [[CrossRef](#)]
52. Białek, J.; Bujalski, W.; Wojdan, K.; Guzek, M.; Kurek, T. Dataset level explanation of heat demand forecasting ANN with SHAP. *Energy* **2022**, *261*, 125075. [[CrossRef](#)]

53. Peng, J.; Dan, Y.; Qiao, R.; Liu, Y.; Dong, J.; Wu, J. How to quantify the cooling effect of urban parks? Linking maximum and accumulation perspectives. *Remote Sens. Environ.* **2021**, *252*, 112135. [CrossRef]
54. Cai, Z.; Han, G.; Chen, M. Do water bodies play an important role in the relationship between urban form and land surface temperature? *Sustain. Cities Soc.* **2018**, *39*, 487–498. [CrossRef]
55. Kang, Z.; Liu, H.; Lu, Y.; Yang, X.; Zhou, X.; An, J.; Yan, D.; Jin, X.; Shi, X. A novel approach to examining the optimal use of the cooling effect of water bodies in urban planning. *Build. Environ.* **2023**, *243*, 110673. [CrossRef]
56. Yao, L.; Sailor, D.J.; Yang, X.; Xu, G.; Zhao, L. Are water bodies effective for urban heat mitigation? Evidence from field studies of urban lakes in two humid subtropical cities. *Build. Environ.* **2023**, *245*, 110860. [CrossRef]
57. Liu, Z.; Cheng, W.; Jim, C.Y.; Morakinyo, T.E.; Shi, Y.; Ng, E. Heat mitigation benefits of urban green and blue infrastructures: A systematic review of modeling techniques, validation and scenario simulation in ENVI-met V4. *Build. Environ.* **2021**, *200*, 107939. [CrossRef]
58. Lin, W.; Yu, T.; Chang, X.; Wu, W.; Zhang, Y. Calculating cooling extents of green parks using remote sensing: Method and test. *Landsc. Urban Plan.* **2015**, *134*, 66–75. [CrossRef]
59. Du, C.; Song, P.; Wang, K.; Li, A.; Hu, Y.; Zhang, K.; Jia, X.; Feng, Y.; Wu, M.; Qu, K.; et al. Investigating the Trends and Drivers between Urbanization and the Land Surface Temperature: A Case Study of Zhengzhou, China. *Sustainability* **2022**, *14*, 13845. [CrossRef]
60. Du, C.; Jia, W.; Chen, M.; Yan, L.; Wang, K. How can urban parks be planned to maximize cooling effect in hot extremes? Linking maximum and accumulative perspectives. *J. Environ. Manag.* **2022**, *317*, 115346. [CrossRef]
61. Yang, Q.; Huang, X.; Yang, J.; Liu, Y. The relationship between land surface temperature and artificial impervious surface fraction in 682 global cities: Spatiotemporal variations and drivers. *Environ. Res. Lett.* **2021**, *16*, 024032. [CrossRef]
62. Ghosh, S.; Kumar, D.; Kumari, R. Assessing spatiotemporal variations in land surface temperature and SUHI intensity with a cloud based computational system over five major cities of India. *Sustain. Cities Soc.* **2022**, *85*, 104060. [CrossRef]
63. Park, J.; Kim, J.-H.; Lee, D.K.; Park, C.Y.; Jeong, S.G. The influence of small green space type and structure at the street level on urban heat island mitigation. *Urban For. Urban Green.* **2017**, *21*, 203–212. [CrossRef]
64. Oliveira, S.; Andrade, H.; Vaz, T. The cooling effect of green spaces as a contribution to the mitigation of urban heat: A case study in Lisbon. *Build. Environ.* **2011**, *46*, 2186–2194. [CrossRef]
65. Qian, Y.; Zhou, W.; Yu, W.; Pickett, S.T.A. Quantifying spatiotemporal pattern of urban greenspace: New insights from high resolution data. *Landsc. Ecol.* **2015**, *30*, 1165–1173. [CrossRef]
66. Zhou, W.; Wang, J.; Cadenasso, M.L. Effects of the spatial configuration of trees on urban heat mitigation: A comparative study. *Remote Sens. Environ.* **2017**, *195*, 1–12. [CrossRef]
67. Shangqiu City Master Plan (2015–2030). Available online: <https://www.shangqiu.gov.cn/zwgk> (accessed on 11 June 2024).
68. Vaz Monteiro, M.; Doick, K.J.; Handley, P.; Peace, A. The impact of greenspace size on the extent of local nocturnal air temperature cooling in London. *Urban For. Urban Green.* **2016**, *16*, 160–169. [CrossRef]
69. Zhou, W.; Huang, G.; Cadenasso, M.L. Does spatial configuration matter? Understanding the effects of land cover pattern on land surface temperature in urban landscapes. *Landsc. Urban Plan.* **2011**, *102*, 54–63. [CrossRef]
70. Masoudi, M.; Tan, P.Y. Multi-year comparison of the effects of spatial pattern of urban green spaces on urban land surface temperature. *Landsc. Urban Plan.* **2019**, *184*, 44–58. [CrossRef]
71. Li, X.; Zhou, W.; Ouyang, Z.; Xu, W.; Zheng, H. Spatial pattern of greenspace affects land surface temperature: Evidence from the heavily urbanized Beijing metropolitan area, China. *Landsc. Ecol.* **2012**, *27*, 887–898. [CrossRef]
72. Maimaitiyiming, M.; Ghulam, A.; Tiyyip, T.; Pla, F.; Latorre-Carmona, P.; Halik, Ü.; Sawut, M.; Caetano, M. Effects of green space spatial pattern on land surface temperature: Implications for sustainable urban planning and climate change adaptation. *ISPRS J. Photogramm. Remote Sens.* **2014**, *89*, 59–66. [CrossRef]
73. Shashua-Bar, L.; Hoffman, M.E. Vegetation as a climatic component in the design of an urban street: An empirical model for predicting the cooling effect of urban green areas with trees. *Energy Build.* **2000**, *31*, 221–235. [CrossRef]
74. Qiu, G.Y.; Zou, Z.; Li, X.; Li, H.; Guo, Q.; Yan, C.; Tan, S. Experimental studies on the effects of green space and evapotranspiration on urban heat island in a subtropical megacity in China. *Habitat Int.* **2017**, *68*, 30–42. [CrossRef]
75. O'Malley, C.; Piroozfar, P.; Farr, E.R.P.; Pomponi, F. Urban Heat Island (UHI) mitigating strategies: A case-based comparative analysis. *Sustain. Cities Soc.* **2015**, *19*, 222–235. [CrossRef]
76. Yang, G.; Yu, Z.; Jørgensen, G.; Vejre, H. How can urban blue-green space be planned for climate adaption in high-latitude cities? A seasonal perspective. *Sustain. Cities Soc.* **2020**, *53*, 101932. [CrossRef]
77. Du, H.; Song, X.; Jiang, H.; Kan, Z.; Wang, Z.; Cai, Y. Research on the cooling island effects of water body: A case study of Shanghai, China. *Ecol. Indic.* **2016**, *67*, 31–38. [CrossRef]
78. Manoli, G.; Fatichi, S.; Schlöpfer, M.; Yu, K.; Crowther, T.W.; Meili, N.; Burlando, P.; Katul, G.G.; Bou-Zeid, E. Magnitude of urban heat islands largely explained by climate and population. *Nature* **2019**, *573*, 55–60. [CrossRef]
79. Zhou, D.; Bonafoni, S.; Zhang, L.; Wang, R. Remote sensing of the urban heat island effect in a highly populated urban agglomeration area in East China. *Sci. Total Environ.* **2018**, *628–629*, 415–429. [CrossRef]
80. Yu, Z.; Xu, S.; Zhang, Y.; Jørgensen, G.; Vejre, H. Strong contributions of local background climate to the cooling effect of urban green vegetation. *Sci. Rep.* **2018**, *8*, 6798. [CrossRef] [PubMed]
81. Forman, R.T.T. *Urban Ecology: Science of Cities*; Cambridge University Press: Cambridge, UK, 2014; ISBN 978-1-107-00700-0.

82. Kong, F.; Sun, C.; Liu, F.; Yin, H.; Jiang, F.; Pu, Y.; Cavan, G.; Skelhorn, C.; Middel, A.; Dronova, I. Energy saving potential of fragmented green spaces due to their temperature regulating ecosystem services in the summer. *Appl. Energy* **2016**, *183*, 1428–1440. [[CrossRef](#)]
83. Seddon, N. Harnessing the potential of nature-based solutions for mitigating and adapting to climate change. *Science* **2022**, *376*, 1410–1416. [[CrossRef](#)]
84. Jaganmohan, M.; Knapp, S.; Buchmann, C.M.; Schwarz, N. The Bigger, the Better? The Influence of Urban Green Space Design on Cooling Effects for Residential Areas. *J. Environ. Qual.* **2016**, *45*, 134–145. [[CrossRef](#)]
85. Aram, F.; Higuera García, E.; Solgi, E.; Mansournia, S. Urban green space cooling effect in cities. *Heliyon* **2019**, *5*, e01339. [[CrossRef](#)] [[PubMed](#)]
86. Newman, P. Cool planning: How urban planning can mainstream responses to climate change. *Cities* **2020**, *103*, 102651. [[CrossRef](#)]
87. Jamei, E.; Rajagopalan, P.; Seyedmahmoudian, M.; Jamei, Y. Review on the impact of urban geometry and pedestrian level greening on outdoor thermal comfort. *Renew. Sustain. Energy Rev.* **2016**, *54*, 1002–1017. [[CrossRef](#)]
88. Wang, Q.; Wang, X.; Zhou, Y.; Liu, D.; Wang, H. The dominant factors and influence of urban characteristics on land surface temperature using random forest algorithm. *Sustain. Cities Soc.* **2022**, *79*, 103722. [[CrossRef](#)]
89. Hou, J.; Rios, M. Community-Driven Place Making. *J. Archit. Educ.* **2003**, *57*, 19–27. [[CrossRef](#)]

Disclaimer/Publisher’s Note: The statements, opinions and data contained in all publications are solely those of the individual author(s) and contributor(s) and not of MDPI and/or the editor(s). MDPI and/or the editor(s) disclaim responsibility for any injury to people or property resulting from any ideas, methods, instructions or products referred to in the content.